




# Continuous wave tunable laser from 616 nm to 637 nm based on a compact sum frequency generation setup

RUIZHE GU,<sup>1</sup> DIA DARWICH,<sup>2</sup>  GERMAIN GUIRAUD,<sup>2</sup>  
MATHIEU CHAUVET,<sup>3</sup> COLINE MAHOB,<sup>4,5</sup> CHRISTOF JANSSEN,<sup>4</sup>  
GIORGIO SANTARELLI,<sup>1</sup>  AND ADELE HILICO<sup>1,6,\*</sup>

<sup>1</sup>LP2N, IOGS, CNRS and Université de Bordeaux, rue François Mitterrand, 33400 Talence, France

<sup>2</sup>Toptica Photonics SAS, 11 Avenue de Canteranne, 33600 Pessac, France

<sup>3</sup>Université Marie & Louis Pasteur, CNRS, institut FEMTO-ST, 25000 Besançon, France

<sup>4</sup>Sorbonne Université, CNRS, MONARIS, 75252 Paris, France

<sup>5</sup>LUX, Observatoire de Paris, Université PSL, Sorbonne Université, CNRS, 75005 Paris, France

<sup>6</sup>Laboratoire de Physique des Lasers, Université Sorbonne Paris Nord, CNRS, 93430 Villetaneuse, France

\*adele.hilico@univ-paris13.fr

**Abstract:** We report on a compact sum frequency generation (SFG) setup generating continuously tunable single-frequency visible radiation from 616 nm to 637 nm, starting from two tunable laser sources at 1  $\mu\text{m}$  and 1.5  $\mu\text{m}$ . We compare two types of crystals: periodically poled lithium niobate (PPLN) and periodically poled magnesium oxide-doped lithium niobate (PPMgOLN), both custom-made such that the tunability range is achieved via temperature control only. We achieve a Watt level of power over the entire tunability range in PPMgOLN, with a mode profile enabling 80% coupling efficiency in a single-mode fiber, limited by the IR sources' tunability, while keeping the system easy to operate.

Published by Optica Publishing Group under the terms of the [Creative Commons Attribution 4.0 License](https://creativecommons.org/licenses/by/4.0/). Further distribution of this work must maintain attribution to the author(s) and the published article's title, journal citation, and DOI.

## 1. Introduction

The development of a high-power single-frequency laser with wavelength emission between 600 nm and 640 nm is important for applications such as single molecule spectroscopy [1], diamond defects spectroscopy [2] and holography [3,4]. It also holds strong potential for ultraviolet (UV) generation, which can be used in Raman [5], fluorescence spectroscopy [6], atmospheric trace gas detection and air quality monitoring (such as OH [7], SO<sub>2</sub> [8] and HOCO [9]) and further for probing the absorption features of atmospheric ozone [10]. Conventional visible CW laser sources such as dye lasers offer broad tunability but are typically bulky, maintenance-intensive, and lack long-term stability [11]. Non-linear frequency generation has emerged as a compelling alternative. However, realizing both broad tunability and watt-level single-frequency output in a compact footprint remains a challenge. Such power level can be achieved by Sum Frequency Generation (SFG, [12]) in cavity housed nonlinear crystals or optical parametric oscillators (OPO, [13]), but the cavity lock leads to a step wavelength tunability and a broad tunability requires complicated electronics. An attractive alternative is the use of high-power infrared (IR) sources and a non-linear crystal for SFG in a single pass configuration enabling narrow-linewidth visible emission.

Among the different types of nonlinear crystals, periodically poled crystals are attractive because they enable type-0 quasi-phase matching (QPM) process without the need for critical phase-matching, although the interacting waves must maintain vertical polarization [14,15]. The phase velocity mismatch can be finely tuned by modifying the crystal temperature and it

enables the possibility to use long crystals without walk-off enabling efficient power generation of CW emission. Periodically poled congruent lithium niobate (PPLN) crystals are particularly advantageous in our wavelength range because of high nonlinear coefficients (e.g.  $d_{33} = 27$  pm/V in LiNbO<sub>3</sub>) compared to other available periodically poled nonlinear crystals such as stoichiometric LiTaO<sub>3</sub> (PPSLT) or KTiOPO<sub>4</sub> (PPKTP) [16]. PPLN crystals can be subject to photorefractive effects (PRE) from 400 to 800 nm at high-power light generation, and is much stronger for generation of shorter wavelengths [17–19]. To mitigate the PRE, LiNbO<sub>3</sub>-based devices are typically operated at elevated temperatures (above 100 °C), or additional doping elements are introduced in LiNbO<sub>3</sub> [20,21], such as in 5% magnesium oxide periodically poled lithium niobate crystal (PPMgOLN). Even though these crystals are really promising, their tunability range is typically limited to 6 to 8 nm by the accessible temperature (from 30 °C to 250 °C) in a uniform crystal. To enhance the different need of tunability/power criteria, multiple types of periodically poled grating structures are available, including uniform [22], chirped [23], cascaded [24] and fan-out structures [25]. We previously demonstrated a tunability of 14 nm using two different channels of a commercial uniform crystal, [26], and Wu et. al [22] produced 60 mW from 560 nm to 630 nm using a broad linewidth Random Raman laser and 10 different channels of a PPLN crystal. Both of these systems require a crystal translation, making it impractical for robustness and packaging. Recent advancements incorporating cascaded poling structures in PPMgOLN have expanded the tunability range of temperature-based phase-matching. Choge et al. [27] demonstrated the simultaneous generation of SFG and SHG with a single pass configuration in a 50 mm PPMgOLN crystal. They have focused a single frequency laser source at 974 nm and a C-band amplified spontaneous emission (ASE) source at the center of the crystal and they have achieved 10%/W and 20.3%/W in conversion efficiency for the SHG and SFG signals, corresponding to powers of 5.2 mW and 9.3 mW, respectively. In [28] the same research group has demonstrated an overall SFG conversion efficiency of 10.4%/W with a 50 mm PPMgOLN crystal combined with a 20 mm step-chirped PPLN crystal as a cascaded module, reaching mW level in tunable orange light with the same sources.

In this work, we study two types of cascaded crystals: a PPLN and a PPMgOLN crystal. The crystals cascade two different poling periods, which allows for broadband QPM via temperature control only. This eliminates the need for mechanical adjustments while tuning the wavelength, making the system highly stable and simple to operate. Notably, this method offers significant time savings when frequent wavelength adjustments that are required throughout spectroscopy experiments. We generate light from 616 nm to 637 nm by coupling 1  $\mu$ m and 1.5  $\mu$ m pumps high power pumps in single pass, achieving output power of up to 1 W.

## 2. Phase-matching condition calculation

To fulfill the type-0 QPM configuration ( $e + e \rightarrow e$ ) for SFG process, the wavevector of three interacting signals, involving the two pump beams ( $k_{1\mu\text{m}}$  and  $k_{1.5\mu\text{m}}$ ) as well as SFG signal ( $k_{\text{SFG}}$ ) need to satisfy the following equation:

$$\Delta k \sim 0 = k_{1\mu\text{m}} + k_{1.5\mu\text{m}} + \frac{2\pi}{\Lambda} - k_{\text{SFG}} \quad (1)$$

where  $k = \frac{2\pi n(\lambda, T)}{\lambda}$ ,  $\Lambda$  is the grating period of the nonlinear crystal, and  $n(\lambda, T)$  is the temperature dependent optical refractive index at given wavelength, which can be calculated using Sellmeier equation [29,30]. In this article,  $n(\lambda, T)$  is specified to be an extraordinary index and under optimal conditions, the SFG wavevector can be described as:

$$\frac{2\pi n_{\text{SFG}}^e(T)}{\lambda_{\text{SFG}}} = \frac{2\pi n_{1\mu\text{m}}^e(T)}{\lambda_{1\mu\text{m}}} + \frac{2\pi n_{1.5\mu\text{m}}^e(T)}{\lambda_{1.5\mu\text{m}}} + \frac{2\pi}{\Lambda} \quad (2)$$

### 3. Experimental setup

#### 3.1. Description of crystals

Two types of crystals, PPLN and PPMgOLN have been investigated. The PPLN crystal was manufactured by the FEMTO Engineering institute [31] without antireflective (AR) coating, resulting in a 14% loss at each interface for both IR pumps and the visible output. The polling periods are calculated by taking 75 °C as minimum QPM temperature to counteract the appearance of PRE.

The PPMgOLN crystal has been manufactured by the commercial manufacturer (Covesion Ltd.) and has an input AR coating at the pump wavelength 1  $\mu\text{m}$  and 1.5  $\mu\text{m}$  and an output AR coating in the visible range leading to losses of less than 1% only. With the same achievable tunability range, the QPM temperature has been calculated using Eq. (2), which varies from 35 °C to 250 °C.

Both types of crystals are produced from 40 mm long, 10 mm wide and 0.5 mm thick bulk (MgO)LN crystals, compatible with a Covesion oven (Covesion PV40) allowing to tune the crystal temperature from room temperature ( $\sim 22$  °C) up to 250 °C using a temperature controller (Covesion OC2). The poling periods are built along 0.5 mm wide channels separated by 0.25 mm unpoled regions in PPLN and 0.2 mm in PPMgOLN. Different cascaded periodicities are manufactured along a single channel, so as to enable the entire tunability range within a single channel by temperature tuning. The crystal architectures are shown in Fig. 1 and corresponding poling periods ( $\Lambda$ ) calculated using Eq. (2) are given in Table 1. The periods of the different PPLN channels vary slightly from one channel to another and offer redundancy to account for possible fabrication errors. Only three channels have distinct periodicities, while the other three are duplicates added to provide alignment flexibility.

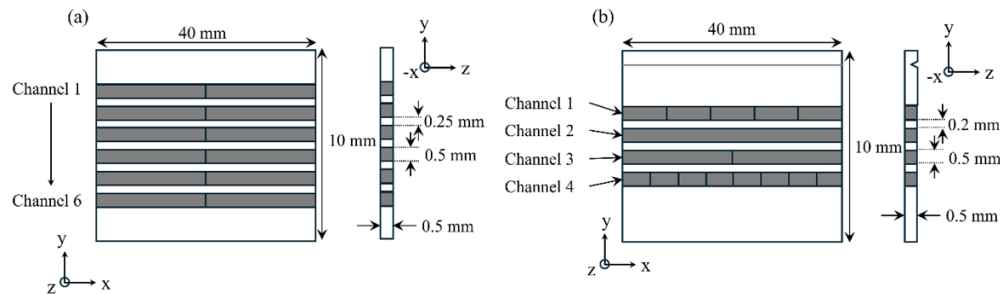


**Fig. 1.** Architectures of (a) the PPLN crystal from FEMTO Engineering institute and (b) the PPMgOLN crystal from Covesion Ltd.

Although we thoroughly investigated all crystal channels, in this article we focus on channels 4 and 5 of the PPLN crystal and channel 3 of the PPMgOLN crystal, which correspond to the best tested periodicities able to generate the visible wavelength from 616 nm to 637 nm.

#### 3.2. Scheme of experimental setup with compact SFG stage

The experimental setup is shown in Fig. 2. The infrared sources consist of two single-frequency tunable high-power sources. A 1  $\mu\text{m}$  continuously tunable single frequency seed (DL Pro from Toptica), emitting around 30 mW from 1030 nm to 1074 nm, is amplified up to 10 W by a homemade two-stages Ytterbium doped fiber amplifier (YDFA). The YDFA is packed in a commercial 3U rack. The 1.5  $\mu\text{m}$  seed laser source consists in a single frequency tunable laser diode (PPCL700 from Pure Photonics) emitting 40 mW of laser radiation from 1533 nm to 1565 nm, which is amplified up to 8 W by an Erbium-Ytterbium doped fiber amplifier (EYDFA)

**Table 1. Periodicity ( $\Lambda$ ) specification in PPLN and PPMgOLN crystals**

Channel No.		PPLN
1	11.15 $\mu\text{m}$	10.7 $\mu\text{m}$
2	11.2 $\mu\text{m}$	10.75 $\mu\text{m}$
3	11.25 $\mu\text{m}$	10.8 $\mu\text{m}$
4	11.15 $\mu\text{m}$	10.7 $\mu\text{m}$
5	11.2 $\mu\text{m}$	10.75 $\mu\text{m}$
6	11.25 $\mu\text{m}$	10.8 $\mu\text{m}$
		PPMgOLN
1	11.94 $\mu\text{m}$ , 12.01 $\mu\text{m}$ , 12.08 $\mu\text{m}$ , 12.15 $\mu\text{m}$ and 12.22 $\mu\text{m}$ of 8 mm length each	
2	11.94 $\mu\text{m}$	
3	11.08 $\mu\text{m}$ , 11.65 $\mu\text{m}$ of 20 mm length each	
4	11.08 $\mu\text{m}$ , 11.65 $\mu\text{m}$ interleaved each 5 mm long	

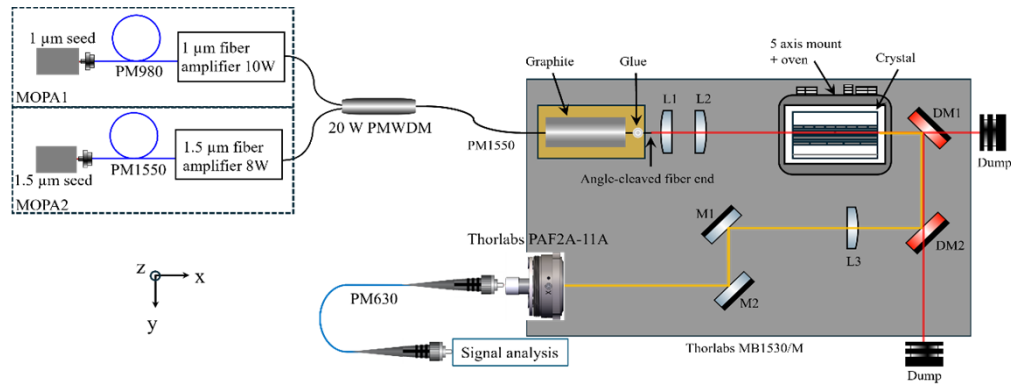


**Fig. 2.** Top view of the SFG experimental setup. MOPA stands for master oscillator power amplifier, and refers to the pump system, which includes the seed laser source and its corresponding fiber amplifier, designated as MOPA1 at 1  $\mu\text{m}$  and MOPA2 at 1.5  $\mu\text{m}$ . The PMWDM is a polarization maintaining wavelength division multiplexer. L1 is an achromatic collimation lens with focal length of 10 mm, L2 is an achromatic doublet with  $f = 100$  nm, L3 is a plano-convex lens with  $f = 150$  mm. DM1 and DM2 are long pass dichroic mirrors (DMLP900) with high transmission beyond 900 nm and high reflection below 900 nm. M1 and M2 are uncoated silver mirrors.

housed in a second 3U rack [32]. The SFG of these two sources enable to generate visible light between 616 nm and 637 nm.

The optical setup for SFG is mounted on an aluminum breadboard with dimensions of 150 mm  $\times$  300 mm  $\times$  12.7 mm in dimensions (Thorlabs MB1530/M, as depicted by the grey area in Fig. 2). The two IR sources are combined using a high-power handling (20 W) polarization maintaining wavelength division multiplexer (PMWDM), ensuring an optimum transverse overlapping of the modes, reducing the number of required lenses and mirrors. The length of the fibers at the input and the output of the PMWDM (1 m of PM1550 fiber) are optimized to avoid the stimulated Brillouin scattering (SBS) of the 1  $\mu\text{m}$  signal propagating inside PM1550 fiber while keeping enough flexibility to easily move the setup on an optical table. To prevent spurious reflections, the end-facet of the PM1550 fiber is cleaved with an 8° angle. To fulfill the type-0 QPM configuration, the slow axis of the PM1550 fiber (along which the polarization of the two pump beams propagate in the fiber) at the output of WDM is aligned with the extraordinary axis

of the PPLN crystals and glued on a copper support. A graphite layer protects the fiber and helps the thermal dissipation. The fiber tip height is aligned with the center of the crystal.

The optical path of the pump beams is shown as red line in Fig. 2, and the SFG signal is displayed as orange line. The IR beams are focused in the crystal using two lenses only, L1 and L2. Their choice results from a tradeoff between commercial availability, space consumption and achromaticity. The common fiber ensures an almost perfect transverse overlap of the beams.

According to Boyd and Kleinman's theory [33], the efficiency of the SFG process depends on the focusing parameter  $\xi = L/b$ , where  $L$  is the length of the crystal and  $b$  the confocal parameter in the crystal with the optimal condition  $\xi = 2.84$ . The first achromatic lens L1 ( $f = 10$  mm) collimates the IR beams. The beam diameters are measured after L1 using a silicon CMOS camera (Ophir SP932U,  $3.45\ \mu\text{m} \times 3.45\ \mu\text{m}$  pixel size) for  $1\ \mu\text{m}$ , giving a value of  $1.7$  mm, and using an InGaAs camera (Widy SWIR 320U,  $25\ \mu\text{m} \times 25\ \mu\text{m}$  pixel size) for  $1.5\ \mu\text{m}$  yielding  $3.7$  mm. The distance between the oven and achromatic doublet L2 has been optimized to focus the IR beams in the center of the crystal. The beams waists diameters have been determined by measuring the caustics with the cameras to be  $75\ \mu\text{m}$  for the  $1\ \mu\text{m}$  signal and  $71\ \mu\text{m}$  for the  $1.5\ \mu\text{m}$  signal, leading to corresponding focusing parameters of  $2.2$  and  $3.7$  when using the extraordinary refractive index calculated using the Sellmeier equation [29,30]. The focus plans in the air are separated by  $3$  mm.

The two dichroic mirrors DM1 and DM2 (DMLP900) are used to separate the pumps from the SFG power, with an average transmission coefficient over  $90\%$  for the IR signal and a reflection coefficient over  $95\%$  for the visible signal. The lens L3 ( $f = 150$  mm) collimates the SFG signal which is reinjected into a PM630 fiber using a Thorlabs commercial fiberport collimator (Thorlabs PAF2A-11A).

The crystal is placed in an oven for phase matching temperature control, while the oven itself is mounted on a 5-axis compact mount for fine tuning in 3 dimensions as well as in pitch and yaw adjustment. The oven controller allows to heat the crystal from room temperature up to  $250\ ^\circ\text{C}$  with a resolution of  $0.01\ ^\circ\text{C}$  and a maximal ramp rate of  $25\ ^\circ\text{C}\cdot\text{min}^{-1}$  while the cooling process is realized through heat dissipation in air.

## 4. Results and discussion

The PPLN and PPMgOLN chips behaviors are described in this part, and we compare their performances in terms of tunability, power scaling as well as long-term stability.

### 4.1. PPLN crystal

The optimization of the crystal alignment with respect to the IR beams was realized by moving the 5-axis mount, by maximizing the conversion efficiency in channel 4 simultaneously at  $618$  nm and  $628$  nm such as to obtain an efficiency as even as possible over the tunability range. Both wavelengths can be produced at the same temperature (around  $150^\circ\text{C}$ ) in the two poling regions  $\Lambda = 10.7\ \mu\text{m}$  and  $\Lambda = 11.15\ \mu\text{m}$ , respectively. The alignment has been coarsely optimized at low power and then fine optimized at high power. For channel 5, the  $620$  nm and  $630$  nm wavelengths are used for optimizing the alignment. The QPM condition has been investigated with  $16$  W of total IR pump power measured before the oven for channel 4 and 5 of the PPLN crystal, and the results are depicted in Fig. 3.

Figure 3 shows the evolution of the QPM temperature as a function of output SFG wavelength with the combination of IR wavelengths and  $\Lambda$  for generation of  $616.5$  nm,  $625$  nm,  $626$  nm,  $635$  nm and  $636$  nm given in Table 2. The results are consistent with the model provided by the FEMTO Engineering institute. The model discontinuity is related to the wavelength change of the  $1\ \mu\text{m}$  pump. These results demonstrate a continuous tunability range from  $616$  nm to  $636$  nm, just by changing the QPM temperature. A specific turnover wavelength near the center of the

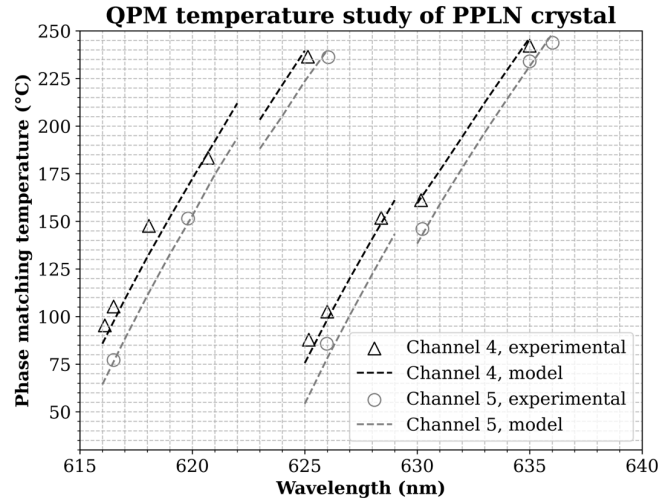


**Fig. 3.** QPM temperature tuning as a function of resulting SFG wavelength in PPLN crystal for channel 4 and 5. The SFG wavelengths have been measured with an optical spectrum analyzer (OSA, YOKOGAWA AQ6374 at a resolution of 0.05 nm). Scatter points correspond to the experimental measurements and dotted curves show the numerical model for channel 4 and 5 respectively.

**Table 2. Optical-to-optical normalized conversion efficiency for different channels in the PPLN crystal.**

Channel 4				
$\lambda_1$ $\mu\text{m}$ (nm)	1030	1050	1050	1070
$\lambda_{1.5}$ $\mu\text{m}$ (nm)	1536	1545	1545	1562
$\lambda_{\text{SFG}}$ (nm)	616.5	625 (236.45 °C)	625 (87.83 °C)	635
$\eta_{\text{Opt-Opt}}$ (%)	4.07	5.56	2.73	8.05
$\eta_{\text{Norm.}}$ (%·W <sup>-1</sup> ·cm <sup>-1</sup> )	0.4	0.4	0.28	0.58
Channel 5				
$\lambda_1$ $\mu\text{m}$ (nm)	1030	1050	1050	1070
$\lambda_{1.5}$ $\mu\text{m}$ (nm)	1536	1550	1550	1565
$\lambda_{\text{SFG}}$ (nm)	616.5	626 (236.17 °C)	626 (85.7 °C)	636
$\eta_{\text{Opt-Opt}}$ (%)	1.96	5.81	2.09	3.93
$\eta_{\text{Norm.}}$ (%·W <sup>-1</sup> ·cm <sup>-1</sup> )	0.17	0.42	0.2	0.28

tunability range, i.e. 625 nm in channel 4 and 626 nm in channel 5, can be obtained with both periodicities when changing temperature.

The power scaling has been performed at 3 chosen wavelengths for each channel, 616.5 nm, 625 nm and 635 nm for channel 4 and 616.5 nm, 626 nm and 636 nm for channel 5. The power is measured directly before the collimator and the beam mode is captured by directing a small portion of the beam to an Ophir SP932U camera. The results are presented in Fig. 4 and the beam modes at turnover wavelength are given in the insets for both temperature configurations and both channels.

Both IR pump beams powers have been incremented equally and simultaneously from 0 to 8.1 W before entering the crystal, corresponding to an increase of IR power from 0 to 7 W inside the crystal, taking into account the Fresnel coefficient loss. The loss of SFG signal due to optics



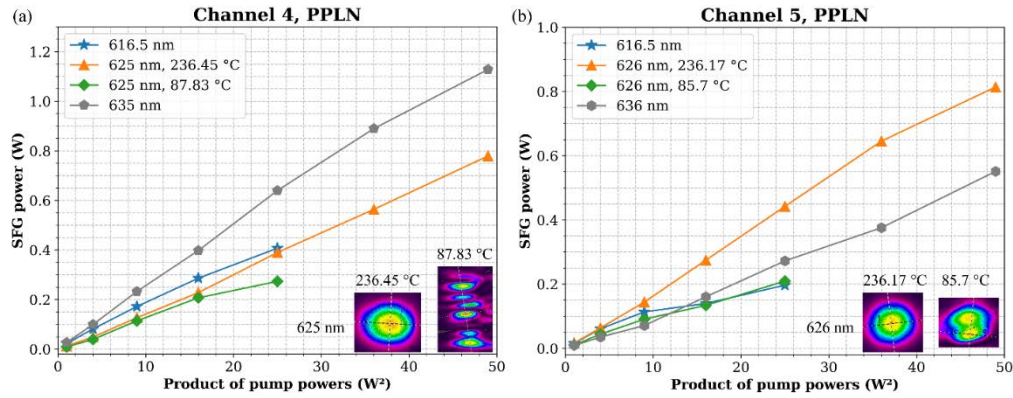


**Fig. 4.** Power scaling of SFG power as a function of the product of the IR pump powers at 616.5 nm (blue), 625 nm (orange for 236.45 °C, green for 87.83 °C) and at 635 nm (grey) with channel 4 in (a); at 616.5 nm (blue), 626 nm (orange for 236.17 °C, green for 85.7 °C) and at 636 nm (grey) with channel 5 in (b) with PPLN crystal. The SFG beam modes are depicted in insets in (a) for 625 nm in channel 4, and in (b) for 626 nm in channel 5.

in the path, including DM1, DM2, L3, M1 and M2, is calculated to be 7%, and it is worth noting that the SFG signal also experiences a Fresnel reflection loss of 14%, which could be reduced by applying an AR treatment to both facets of the crystal. Figure 4 demonstrates the power scaling at the crystal output if AR coating had been added as a function of product of pump power injected into the crystal. For channel 4, at 616.5 nm and at 625 nm (low temperature), the power scaling was stopped by the onset of photorefractive effect occurring when the QPM temperature is below 100 °C, resulting in a SFG power and conversion efficiency drop, as well as a degradation of the SFG beam mode, as shown in the inset in Fig. 4(a). The same issue has been encountered on channel 5.

Both the optical-to-optical conversion efficiency and the normalized optical conversion efficiency have been evaluated. The optical-to-optical conversion efficiency can be calculated using the equation  $\eta_{\text{Opt-Opt}} = P_{\text{SFG}} / (P_{1\mu\text{m}} + P_{1.5\mu\text{m}})$ , with  $P_{\text{SFG}}$  being the power of the SFG signal and  $P_{1\mu\text{m}}$  and  $P_{1.5\mu\text{m}}$  being the power of the pump injected into the crystal. As for the normalized conversion efficiency, we use  $\eta_{\text{Norm.}} = P_{\text{SFG}} / (P_{1\mu\text{m}} \times P_{1.5\mu\text{m}} \times L)$  with  $L$  designating the crystal length. The results are presented in Table 2.

For the PPLN crystals, the experimental results yield maximum output power of 1.13 W (at 635 nm in channel 4) by injecting 14 W of total pump inside the crystal. A maximum  $\eta_{\text{Opt-Opt}}$  of 8%, corresponding to  $\eta_{\text{Norm.}} = 0.58\% \cdot \text{W}^{-1} \cdot \text{cm}^{-1}$ , has been achieved. Despite of compensating the Fresnel coefficient loss, our experimental results give an efficiency smaller than the MgO doped uniform sample ( $2\% \cdot \text{W}^{-1} \cdot \text{cm}^{-1}$ ) [26], and close to the conversion efficiency in a fan-out structure crystal [25]. The efficiencies at low temperatures drops due to PRE. The discrepancy in SFG power can be attributed to several factors: (1) bad centering of the waists focus alongside each cascaded poling region, reducing the efficiency by at least a factor of 2; and (2) spatial walk-off between the beam waist positions of the two pump wavelengths within the crystal.

In conclusion, the tunability range has been achieved with PPLN crystal, but is limited not only by the IR wavelength but also the QPM temperature due to the PRE. One can observe that the slight  $\Lambda$  change between the 2 channels induces a slight change in tunability range while keeping the bandwidth the same. To further mitigate such phenomenon, the PPLN crystal can be replaced to a PPMgOLN crystal.

#### 4.2. PPMgOLN crystal

For the MgO doped crystal, the cascaded periodicities have been chosen so as to cover all of the SFG  $\lambda$  range varying the temperature between 40 °C and 230 °C. The alignment is optimized simultaneously at 619 nm and 633 nm, using the same strategy as for the PPLN crystal. The QPM temperature is evaluated with a total of 14 W of IR pumps injected into the crystal, i.e. 7 W of each pump. The results are shown in Fig. 5 and the detailed SFG condition is given in Table 3. The central wavelength of the tunable range (i.e., 627 nm) can be realized with both poling periods at 39.6 °C and 229.53 °C, showing that our system is completely tunable without additionally mechanical movement of the crystal. In this case, the tunability is limited at high wavelengths by the operational wavelength range of the MOPAs.

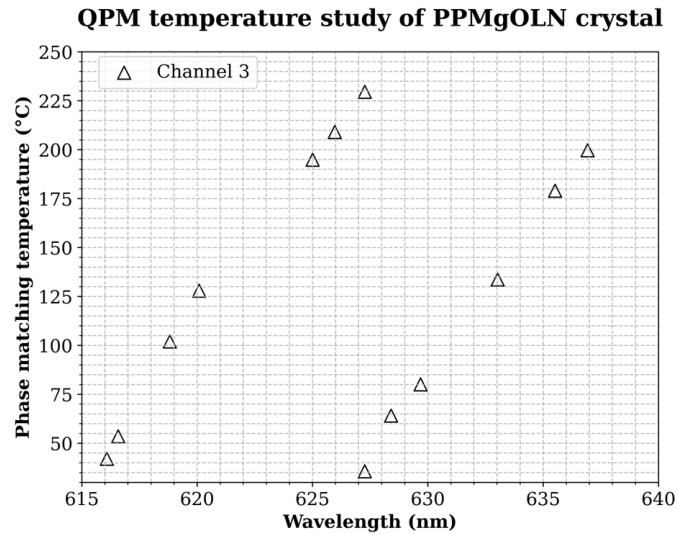


**Fig. 5.** QPM temperature tuning as a function of resulting SFG wavelength in PPMgOLN crystal. The SFG wavelengths have been measured with an optical spectrum analyzer (OSA, YOKOGAWA AQ6374 at a resolution of 0.05 nm).

**Table 3.** Optical-to-optical and normalized SFG conversion efficiency in PPMgOLN crystal.

$\lambda_{1\mu\text{m}}$ (nm)	1030	1050	1050	1070	1074
$\lambda_{1.5\mu\text{m}}$ (nm)	1536	1558	1558	1565	1565
$\lambda_{\text{SFG}}$ (nm)	616.58	627.27 (229.53 °C)	627.27 (39.6 °C)	635.55	636.93
$\eta_{\text{Opt-Opt}}$ (%)	7.17	6.28	9.64	10.14	7.43
$\eta_{\text{Norm.}}$ (%·W <sup>-1</sup> ·cm <sup>-1</sup> )	0.51	0.45	0.67	0.73	0.54

The power scaling of the SFG signal as a function of the product of the IR optical powers is shown on Fig. 6. A maximal SFG power of 1.4 W is achieved, limited only by the available IR optical powers [26] and even a Watt on the all tunability range. The collimated beam profiles at 627.27 nm with two different QPM temperatures are captured using the Ophir SP932U camera and are displayed in the insets in Fig. 6. They show a Gaussian intensity distribution with over 90% of ellipticity with a beam diameter ( $D_{1/e^2}$ ) of 1.8 mm. No beam degradation due to PRE is observed. Similar beam modes have been obtained for other SFG wavelengths.

The optical-to-optical conversion efficiency and the normalized conversion efficiency are listed in Table 3. Compared to the PPLN crystal, higher SFG conversion efficiency is obtained.



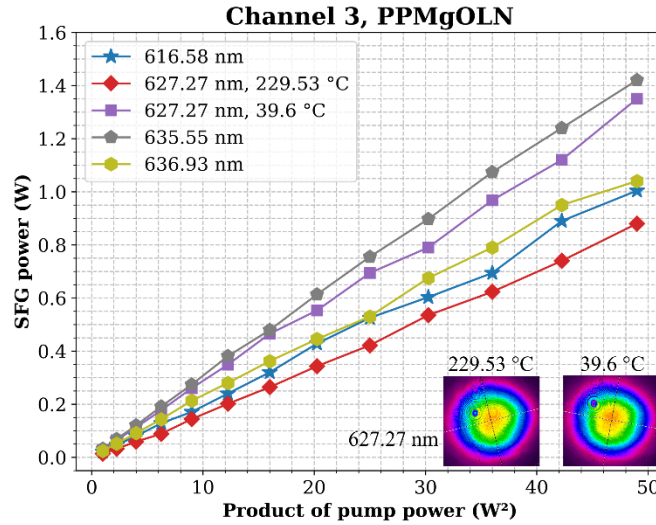


**Fig. 6.** Power scaling measurement of SFG signal as a function of product of IR pump power at 616.58 nm (blue), 627.27 nm (red for 229.53 °C, purple for 39.6 °C), 635.55 nm (grey) and 636.93 nm (yellow) in PPMgOLN.

For a 40 mm long single periodicity PPMgOLN crystal, the theoretical estimation gives  $\eta_{\text{Norm.}} = 3.5\% \cdot \text{W}^{-1} \cdot \text{cm}^{-1}$  under the ideal condition, i.e. undepleted pump beams and optimum focusing parameter according to Boyd and Kleinman's theory [34,35]. This customized crystal shows  $0.45 < \eta_{\text{Norm.}} < 0.73\% \cdot \text{W}^{-1} \cdot \text{cm}^{-1}$  by a factor of 4 less than a MgO doped PPLN with a uniform grating structure [26]. We attribute this to the fact that the crystal behaves as if there were 2 cascaded shorter crystals and only one of them participates to visible light generation, reducing the efficiency by a factor of 2. Moreover, the focus of the IR beams is not centered into these half-crystals, which further reduces the expected efficiency compared to a single periodicity channel. A small fraction of the SFG signal has been analyzed by the YOKOGAWA AQ6374 OSA with a resolution of 0.05 nm. An optical signal to noise ratio (OSNR) over 70 dB has been measured.

To address the long-term stability, endurance tests over 10 hours have been conducted for different wavelength configurations shown in Fig. 7. The discrepancy in power at different SFG wavelengths can be related to the combination of several factors including: (1) the stability of the pump power; (2) thermal fluctuation inside the crystal when working at low QPM temperature and (3) the beam waist position with respect to the different periodicity zone. But the overall fluctuation in SFG power is below 0.8%.

The temperature acceptance study was carried out at 616 nm and a temperature acceptance of 2.3 °C was obtained, compared to 1.1 °C in a single periodicity grating crystal of the same length [26]. The power stability at 616 nm has been measured before and after injection into a PM630 fiber and the results are shown in Fig. 8. The power measurement shows the stability over 10 hours before fiber injection and over 2 hours after the PM630 fiber. An average of 80% coupling efficiency is achieved and a mean power of 0.83 W is measured with fluctuations below 0.6%, indicating SFG signal is obtained with high power stability with high quality beam mode. Although not depicted here, the relative intensity noise of this laser has been studied and shows a similar performance as measured in [26]. The setup maintained excellent optical alignment after being transported from Bordeaux to Paris, requiring only minimal adjustments and thus confirming its outstanding robustness.

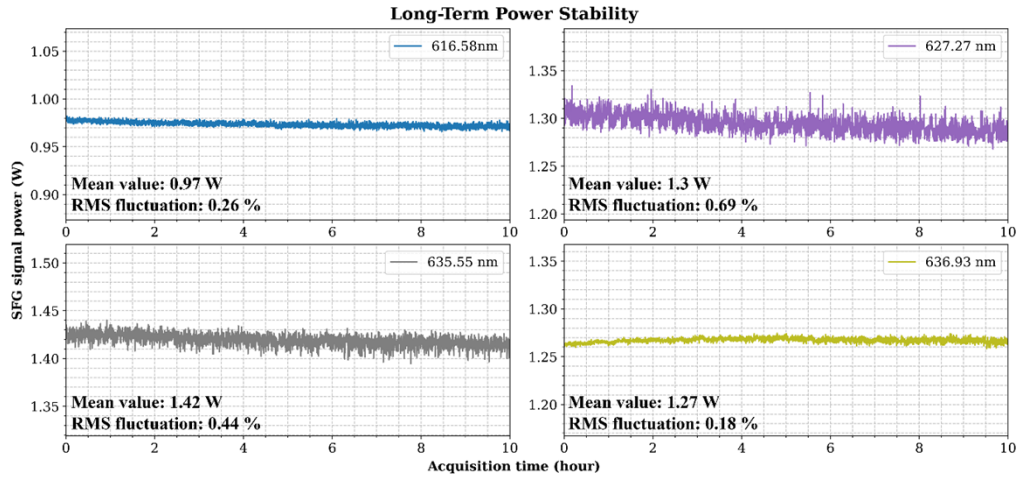


**Fig. 7.** Long-term power stability measurement for different SFG wavelengths. The measurement is performed with collimated SFG signals over 10 hours at optimal power level.

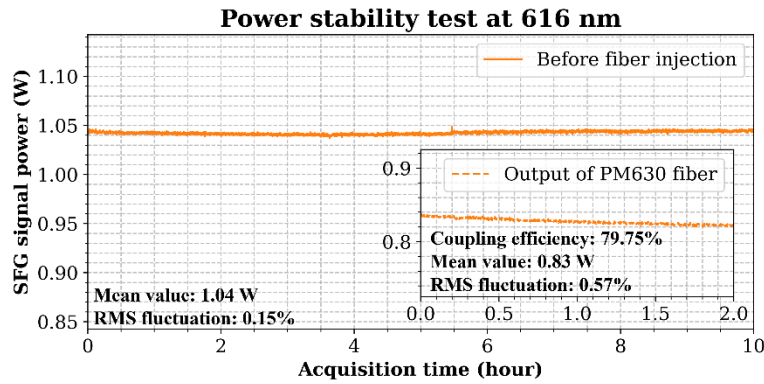


**Fig. 8.** Power stability measurement at 616 nm before and after (inset) the injection in PM630 fiber.

#### 4.3. Summary of CW SFG efficiency and tunabilities in PPMgOLN

A summary of the results discussed in the previous sections is provided in Table 4 and compared to state-of-the-art publications. It summarizes the key performance metrics: nonlinear media, tunability range, power, SFG conversion efficiencies and tuning mechanism across different CW SFG systems.

### 5. Conclusion and perspectives

We have demonstrated a compact, fibered Watt-level continuous-wave laser source tunable from 616 nm to 637 nm based on SFG using custom-engineered cascaded-period PPLN and PPMgOLN crystals. The PPLN crystal performance is limited by PRE at low temperature. With MgO doping, the crystal shows better performance in terms of SFG conversion efficiency, power stability and beam quality. The system relies solely on temperature control to achieve broad and continuous wavelength tuning, eliminating the need for mechanical adjustments or complex alignment procedures. This thermally controlled tuning mechanism greatly simplifies operation

and enhances system robustness, with the tunability range limited only by the available IR input wavelengths.

**Table 4. Summary of reported continuous-wave SFG conversion efficiencies from this work and previous studies. All results correspond to single-pass CW configurations using various structures of nonlinear material.**

Work	Nonlinear medium	SFG wavelength (nm)	Nominal power	$\eta_{\text{Norm.}}$ ( $\% \cdot \text{W}^{-1} \cdot \text{cm}^{-1}$ )	Tuning mechanism
This work	Cascaded 2 poling period PPMgOLN single-crystal	616-637	1 W	0.5-0.8	Solely via temperature and pump wavelength
Wu et al. [22]	Single-period 1 cm PPLN crystal, 10 channels	560-630	70mW	0.15	Tuning via temperature and mechanical translation of crystal
Darwich et al. [26]	Single-period 4 cm PPMgOLN single-crystal, 2 channels	616-630	6.7-7 W	2.5	Tuning via temperature and mechanical translation of crystal
Choge et al. [28]	2 cascaded modules containing PPMgOLN crystal	596.9	10 mW	$10.4\% \cdot \text{W}^{-1}$ (50 mm + 20 mm)	Tuning by varying the crystal position, temperature and etalon tilt angle

The use of a dual-period crystal structure enables efficient phase matching across a wide spectral span via type-0 QPM, while delivering excellent long-term power stability. This performance highlights the suitability of our approach not only for applications in the visible range but also as a promising platform for future development of narrow-linewidth tunable sources in the ultraviolet regime, where SFG can be combined with further nonlinear conversion stages (SHG). Increasing the power of the IR sources to 20 W would allow to generate a tunable single frequency visible source of two Watts. The combination of simplicity, stability, and scalability positions this system as a strong candidate for replacing more complex or less stable visible and UV sources in spectroscopy, sensing, and quantum photonics applications. And this system will be implemented in laboratory experiments involving laser spectroscopy, aimed at measuring the absorption cross-sections of ozone in the Huggins band.

**Funding.** Agence Nationale de la Recherche (ANR-22-CE01-0007, ANR-23-PEEL-0004, ANR-21-ESRE-0040, ANR-17-EURE-0002); Conseil Régional Aquitaine (AAPR2022-2021-17190110 bis); Université de Bordeaux (GPR Light).

**Acknowledgments.** The authors thank Kentin Poncelet for help with the amplifiers and during the setup transportation, Arnaud Tizon, Laurent Gontier and Philippe Teulat for their technical support. We acknowledge the support of the French RENATECH network through its FEMTO-ST technological facility.

**Disclosures.** The authors declare no conflicts of interest.

**Data availability.** Data underlying the results presented in this paper are not publicly available at this time but may be obtained from the authors upon reasonable request.

## References

1. J.-B. Trebbia, P. Tamarat, and B. Lounis, "Indistinguishable near-infrared single photons from an individual organic molecule," *Phys. Rev. A* **82**(6), 063803 (2010).
2. S. Häußler, G. Thiering, A. Dietrich, *et al.*, "Photoluminescence excitation spectroscopy of  $\text{SiV}^-$  and  $\text{GeV}^-$  color center in diamond," *New J. Phys.* **19**(6), 063036 (2017).

3. K. Hens, J. Sperling, B. Sherliker, *et al.*, "Lasers for holographic applications: important performance parameters and relevant laser technologies," in *Practical Holography XXXIII: Displays, Materials, and Applications*, H. I. Bjelkhagen and V. M. Bove, eds. (SPIE, 2019), p. 7.
4. S. Trotzky, A. Mark, N. Waasem, *et al.*, "Mastering challenges in holography with widely tunable CW optical parametric oscillators," in *Practical Holography XXXVI: Displays, Materials, and Applications*, H. I. Bjelkhagen and S.-H. Lee, eds. (SPIE, 2022), p. 15.
5. F. Fan, Z. Feng, and C. Li, "UV Raman spectroscopic study on the synthesis mechanism and assembly of molecular sieves," *Chem. Soc. Rev.* **39**(12), 4794 (2010).
6. B. Gmeiner, A. Maser, T. Utikal, *et al.*, "Spectroscopy and microscopy of single molecules in nanoscopic channels: spectral behavior vs. confinement depth," *Phys. Chem. Chem. Phys.* **18**(29), 19588–19594 (2016).
7. L. Corner, J. S. Gibb, G. Hancock, *et al.*, "Sum frequency generation at 309 nm using a violet and a near-IR DFB diode laser for detection of OH," *Appl. Phys. B: Lasers Opt.* **74**(4-5), 441–444 (2002).
8. G. Somesfalean, Z. G. Zhang, M. Sjöholm, *et al.*, "All-diode-laser ultraviolet absorption spectroscopy for sulfur dioxide detection," *Appl. Phys. B* **80**(8), 1021–1025 (2005).
9. M. Cazorla, G. M. Wolfe, S. A. Bailey, *et al.*, "A new airborne laser-induced fluorescence instrument for in situ detection of formaldehyde throughout the troposphere and lower stratosphere," *Atmos. Meas. Tech.* **8**(2), 541–552 (2015).
10. J. Orphal, J. Staehelin, J. Tamminen, *et al.*, "Absorption cross-sections of ozone in the ultraviolet and visible spectral regions: Status report 2015," *J. Mol. Spectrosc.* **327**, 105–121 (2016).
11. P. Thoumany, T. Hänsch, G. Stania, *et al.*, "Optical spectroscopy of rubidium Rydberg atoms with a 297 nm frequency-doubled dye laser," *Opt. Lett.* **34**(11), 1621 (2009).
12. R. W. Boyd, *Nonlinear Optics*, 4th ed. (Academic Press is an imprint of Elsevier, 2019).
13. J. Sperling, M.-H. Schubert, M. Wenderoth, *et al.*, "Breakthrough instruments and products: Laser light tunable across the visible up to mid-infrared: Novel turnkey cw OPO with efficiency-optimized design," *Rev. Sci. Instrum.* **92**(12), 129502 (2021).
14. D. S. Hum and M. M. Fejer, "Quasi-phases-matching," *C. R. Phys.* **8**(2), 180–198 (2006).
15. J. Yao and Y. Wang, "Quasi-phase-matching technology," in *Nonlinear Optics and Solid-State Lasers*, Springer Series in Optical Sciences (Springer: Berlin Heidelberg, 2012), 164, pp. 319–382.
16. S. Manjorán, H. Zhao, I. T. Lima, *et al.*, "Phase-matching properties of PPKTP, MgO:PPSLT and MgO:PPcLN for ultrafast optical parametric oscillation in the visible and near-infrared ranges with green pump," *Laser Phys.* **22**(8), 1325–1330 (2012).
17. H. B. Serreze and R. B. Goldner, "Study of the wavelength dependence of optically induced birefringence change in undoped LiNbO<sub>3</sub>," *Appl. Phys. Lett.* **22**(12), 626–627 (1973).
18. B. Chen, J. F. Campos, W. Liang, *et al.*, "Wavelength and temperature dependence of photorefractive effect in quasi-phase-matched LiNbO<sub>3</sub> waveguides," *Appl. Phys. Lett.* **89**(4), 043510 (2006).
19. Y. Furukawa, K. Kitamura, A. Alexandrovski, *et al.*, "Green-induced infrared absorption in MgO doped LiNbO<sub>3</sub>," *Appl. Phys. Lett.* **78**(14), 1970–1972 (2001).
20. T. Volk, M. Wöhlecke, and N. Rubinina, "Optical damage resistance in lithium niobate," in *Photorefractive Materials and Their Applications 2*, P. Günter and J.-P. Huignard, eds., Springer Series in Optical Sciences (Springer: New York, 2007), 114, pp. 165–203.
21. C. Cochard, M. Guennou, T. Spielmann, *et al.*, "Effect of optical damage resistant dopants on the dielectric properties of LiNbO<sub>3</sub>: Insight from broadband impedance spectroscopy and Raman scattering," *J. Appl. Phys.* **123**(15), 154105 (2018).
22. H. Wu, W. Wang, B. Hu, *et al.*, "Widely tunable continuous-wave visible and mid-infrared light generation based on a dual-wavelength switchable and tunable random Raman fiber laser," *Photonics Res.* **11**(5), 808 (2023).
23. D. K. Choge, H.-X. Chen, G. Lei, *et al.*, "Tunable multi-color coherent light generation in single MgO: PPLN bulk crystal," (2018).
24. W. R. Bosenberg, J. I. Alexander, L. E. Myers, *et al.*, "25-W, continuous-wave, 629-nm solid-state laser source," *Opt. Lett.* **23**(3), 207 (1998).
25. Y. Wang, Y. Huang, Z. Weng, *et al.*, "Variable wavelength conversion based on fan-out grating in QPM-LN," in (2007), p. 67820F.
26. D. Darwich, R. Prakash, C. Dixneuf, *et al.*, "High power ultralow-intensity noise continuous wave laser tunable from orange to red," *Opt. Express* **30**(8), 12867 (2022).
27. D. Choge, H.-X. Chen, Y.-B. Xu, *et al.*, "Blue and orange two-color CW laser based on single-pass second-harmonic and sum-frequency generation in MgO:PPLN," *Appl. Sci.* **8**(4), 629 (2018).
28. D. Choge, H.-X. Chen, B.-L. Tian, *et al.*, "A tunable CW orange laser based on a cascaded MgO:PPLN single-pass sum-frequency generation module," *Appl. Sci.* **8**(3), 439 (2018).
29. D. H. Jundt, "Temperature-dependent Sellmeier equation for the index of refraction,  $n_e$ , in congruent lithium niobate," *Opt. Lett.* **22**(20), 1553 (1997).
30. O. Gayer, Z. Sacks, E. Galun, *et al.*, "Temperature and wavelength dependent refractive index equations for MgO-doped congruent and stoichiometric LiNbO<sub>3</sub>," *Appl. Phys. B* **91**(2), 343–348 (2008).
31. M. Chauvet, F. Henrot, F. Bassignot, *et al.*, "High efficiency frequency doubling in fully diced LiNbO<sub>3</sub> ridge waveguides on silicon," *J. Opt.* **18**(8), 085503 (2016).

32. D. Darwich, Y.-V. Bardin, M. Goepfner, *et al.*, “Ultralow-intensity noise, 10 W all-fiber single-frequency tunable laser system around 1550 nm,” *Appl. Opt.* **60**(27), 8550 (2021).
33. G. D. Boyd and D. A. Kleinman, “Parametric interaction of focused gaussian light beams,” *J. Appl. Phys.* **39**(8), 3597–3639 (1968).
34. J. Wang, J. Bai, J. He, *et al.*, “Realization and characterization of single-frequency tunable 637.2 nm high-power laser,” *Opt. Commun.* **370**, 150–155 (2016).
35. D. L. Hart, L. Goldberg, and W. K. Burns, “Red light generation by sum frequency mixing of Er/Yb fiber amplifier output in QPM LiNbO<sub>3</sub>,” *Electron. Lett.* **35**(1), 52–53 (1999).